


Article

# Actin Filament in the First Cell Cycle Contributes to the Determination of the Anteroposterior Axis in Ascidian Development

Toshiyuki Goto <sup>1,2</sup>, Shuhe Torii <sup>1</sup>, Aoi Kondo <sup>1</sup>, Kazumasa Kanda <sup>1</sup>, Junji Kawakami <sup>1</sup>, Yosky Kataoka <sup>2,3</sup>   
and Takahito Nishikata <sup>1,\*</sup>

<sup>1</sup> Frontiers of Innovative Research in Science and Technology (FIRST), Konan University, 7-1-20 Minatojima-Minamimachi, Chuo-k, Kobe 650-0047, Japan; d1961001@s.konan-u.ac.jp (T.G.); m2161013@s.konan-u.ac.jp (S.T.); s1891017@s.konan-u.ac.jp (A.K.); kazu186607@gmail.com (K.K.); kawakami@konan-u.ac.jp (J.K.)

<sup>2</sup> Laboratory for Cellular Function Imaging, RIKEN Center for Biosystems Dynamics Research, Kobe 650-0047, Japan; kataokay@riken.jp

<sup>3</sup> RIKEN-JEOL Collaboration Center, Multi-Modal Microstructure Analysis Unit, Kobe 650-0047, Japan

\* Correspondence: nisikata@konan-u.ac.jp; Tel.: +81-78-303-1349

**Abstract:** In many animal species, the body axis is determined by the relocalization of maternal determinants, organelles, or unique cell populations in a cytoskeleton-dependent manner. In the ascidian first cell cycle, the myoplasm, including mitochondria, endoplasmic reticulum (ER), and maternal mRNAs, move to the future posterior side concomitantly (called ooplasmic segregation or cytoplasmic and cortical reorganization). This translocation consists of first and second phases depending on the actin and microtubule, respectively. However, the transition from first to second phase, that is, translocation of myoplasmic components from microfilaments to microtubules, has been poorly investigated. In this study, we analyzed the relationship between these cytoskeletons and myoplasmic components during the first cell cycle and their role in morphogenesis by inhibitor experiments. Owing to our improved visualization techniques, there was unexpected F-actin accumulation at the vegetal pole during this transition period. When this F-actin was depolymerized, the microtubule structure was strongly affected, the myoplasmic components, including maternal mRNA, were mislocalized, and the anteroposterior axis formation was disordered. These results suggested the importance of F-actin during the first cell cycle and the existence of interactions between microfilaments and microtubules, implying the enigmatic mechanism of ooplasmic segregation. Solving this mystery leads us to an improved understanding of ascidian early development.

**Keywords:** axis determination; ER; actin; microtubule; maternal mRNA



**Citation:** Goto, T.; Torii, S.; Kondo, A.; Kanda, K.; Kawakami, J.; Kataoka, Y.; Nishikata, T. Actin Filament in the First Cell Cycle Contributes to the Determination of the Anteroposterior Axis in Ascidian Development. *J. Dev. Biol.* **2022**, *10*, 10. <https://doi.org/10.3390/jdb10010010>

Academic Editors: Tsutomu Nohno and Hideyo Ohuchi

Received: 6 December 2021

Accepted: 2 February 2022

Published: 4 February 2022

**Publisher's Note:** MDPI stays neutral with regard to jurisdictional claims in published maps and institutional affiliations.



**Copyright:** © 2022 by the authors. Licensee MDPI, Basel, Switzerland. This article is an open access article distributed under the terms and conditions of the Creative Commons Attribution (CC BY) license (<https://creativecommons.org/licenses/by/4.0/>).

## 1. Introduction

Maternal mRNA, which is produced from the maternal genome during oogenesis, is indispensable for body planning in many animal species. The localization and translation of maternal mRNA is strictly regulated during early embryogenesis. For the correct localization of maternal mRNA, cytoskeletons play a crucial role in the transport and anchoring of some animal eggs such as flog (cortical rotation) [1,2], teleost fish (cortical rotation) [3], and nematodes (cytoplasmic flow) [4,5].

Ascidian (Chordata) unfertilized eggs have a unique cytoplasm, designated as myoplasm, which consists of mitochondria-rich cytoplasm (MRC), cortical endoplasmic reticulum (cER), and maternal mRNAs called postplasmic/PEM RNAs [6,7]. In the first cell cycle, the myoplasm shows dynamic movement toward the future posterior side (called ooplasmic segregation or cytoplasmic and cortical reorganization) [8], and is important for anteroposterior axis formation [7].

This ooplasmic segregation consists of two phases. In the first phase, fertilization triggers the contraction of cortical actin filaments to the vegetal pole and the concentration of the myoplasm at the vegetal pole [9–11]. This first phase is completed within 5 min postfertilization (mpf). During the second phase, growing sperm aster migrates from the vegetal pole to the posterior side along the egg cortex, and finally, the sperm nucleus enters the center of the egg to fuse with the female nucleus [8]. The myoplasm moves toward the posterior pole following this sperm-aster movement and depends on the microtubules [9–11]. We recently reported the cortical array of microtubules in the posterior–vegetal region (CAMP) during the second phase, suggesting the importance of myoplasm translocation [12,13]. This second phase of ooplasmic segregation occurs roughly from 30 to 45 mpf. Although these two phases of ooplasmic segregations are well-described, the mechanisms of transition between the first and second phases are poorly understood. One of the concerns is how the myoplasm switches its chariot from F-actin to the microtubule.

Previously, cER and postplasmic/PEM mRNAs were thought to move posteriorly together during the second phase [7,8]. However, our recent observations showed that before the second phase, some postplasmic/PEM mRNAs dissociated from dense ER, which corresponds to the cER with a more deeply expanded ER mass [14]. Moreover, they reassembled by the four-cell stage and subsequently inherited in the centrosome attracting body (CAB) [14]. CAB is responsible for unequal cleavage and determines the anteroposterior axis [15,16]. These results strongly suggest the existence of unexpected mechanisms between the first and second phases of ooplasmic segregations and their importance for the anteroposterior axis formation.

In this study, owing to the improvement and refinement of the entire process of visualization techniques, we succeeded in revealing the prolonged F-actin accumulation at the vegetal pole up to 30 mpf. We analyzed the role of actin filaments during the first cell cycle on the segregation of myoplasm, including CAMP formation, translocation of macho-1, dense ER, and mitochondria and axis determination. The importance of the relationship between actin filaments and microtubules will be discussed.

## 2. Materials and Methods

### 2.1. Animal Experiments

Ascidian (*Ciona intestinalis* type A; also called *Ciona robusta*) adults were obtained from the National BioResource Project (NBRP), Tokyo, Japan. Methods for egg and sperm handling, fertilization, and dechoriation were performed as described previously [17,18]. The embryos were reared in filtered seawater at 18 °C. At this temperature, the first and second phase of ooplasmic segregations start immediately after fertilization and from approximately 30 min postfertilization (mpf), respectively. The first cleavage occurs at approximately 60 mpf. In the inhibitor experiments, eggs were treated with 2 µg/mL cytochalasin B (CytB; Sigma-Aldrich, St. Louis, MO, USA), 2.5 µg/mL nocodazole (Noco; Sigma-Aldrich), or the same dilution of solvent (0.1% DMSO) as a control during the desired periods. The eggs were exposed to these inhibitors with 3 mL seawater. Then, eggs were replaced to 10 mL seawater and washed 5 times with fresh seawater. It has been reported that cortical F-actin in CytB-treated culture cells could be recovered within 5 min after washout with this protocol [19].

### 2.2. Whole-Mount Immunofluorescent Staining

For microtubule staining, dechorionated *Ciona* eggs/embryos were fixed with 100% methanol at room temperature (approximately 25 °C) for 1 h. The fixed specimens were treated with ethanol up series (35%, 70%, and 100%) and stored at −30 °C until further use. After washing with phosphate-buffered saline containing 0.05% Tween 20 (PBST), the specimens were treated with G1T0 (4 mol/L urea (MP Biomedicals, Santa Ana, CA, USA), and 1% glycerol in distilled water) for 90 min at 4 °C [12].

For double staining of the ER and microtubules, dechorionated *Ciona* eggs and embryos were fixed with Cold-Fix solution (3.2% formaldehyde in 80% methanol) at −30 °C for

1 h, followed by continued fixation at room temperature for 1 h with gentle shaking every 20 min. Both types of fixed specimens were treated with ethanol up series (35%, 70%, and 100%) and stored at  $-30^{\circ}\text{C}$  until further use. After washing with PBST, the specimens were treated with G1T0 for 90 min at  $4^{\circ}\text{C}$  and then treated with antigen retrieval solution (modified from Hayashi et al., 2011; 6 M urea and 0.1 M Tris-HCl, pH 9.5) [20] for 30 min at  $80^{\circ}\text{C}$ . The specimens were immunostained with the following antibodies: anti- $\alpha$ -tubulin mouse monoclonal antibody (anti-microtubule antibody; clone DM1A; Sigma-Aldrich; 1:100 dilution), anti-glucose-regulated protein 78 (GRP78; also known as Bip) rabbit polyclonal antibody (anti-ER antibody; StressMarq Biosciences, Victoria, BC, Canada; 1:100 dilution), Alexa Fluor 488-conjugated goat anti-mouse IgG antibody (Thermo Fisher Scientific; 1:1000 dilution), and Alexa Fluor Plus 555-conjugated goat anti-rabbit IgG antibody (Thermo Fisher Scientific; 1:1000 dilution). Nuclei were stained with  $5\ \mu\text{g}/\text{mL}$  4',6-diamidino-2-phenylindole dihydrochloride (DAPI). The stained specimens were then mounted with methyl salicylate (Nacalai Tesque, Kyoto, Japan).

### 2.3. Phalloidin Staining

For F-actin staining, dechorionated *Ciona* eggs/embryos were fixed with a 1:1 mixed solution of extraction buffer (2% Triton-X 100, 50 mM  $\text{MgCl}_2$ , 10 mM KCl, 10 mM EGTA, 20% glycerol, 25 mM imidazole) and fixation buffer (0.25% glutaraldehyde (Nacalai Tesque), 3.7% formaldehyde, 100 mM HEPES (pH = 7.0), 50 mM EGTA, 10 mM  $\text{MgSO}_4$ , and 525 mM sucrose) [21] for 15 min at room temperature. This was followed by continued fixation in fixation buffer for 2 h at room temperature. The fixed specimens were washed with PBST and treated with 10 unit/mL Alexa Fluor 488-labeled phalloidin (Molecular Probes, Eugene, OR, USA) for 30 min at room temperature. For clearing without dehydration, stained specimens were treated with 40% fructose (Fujifilm-Wako, Tokyo, Japan) for 30 min at room temperature and then mounted in SeeDB (80.2% wt/wt fructose, 0.5%  $\alpha$ -thioglycerol) [22].

### 2.4. Whole-Mount RNA In Situ Hybridization

Dechorionated *Ciona* eggs/embryos were fixed with a Cold-Fix solution. Fixed specimens were treated with 0.2% Triton-X 100 for 10 min at room temperature and then fixed with paraformaldehyde for 1 h at room temperature. The postfixed specimens were treated with 0.1 M 2,2',2'-nitriлотriethanol (Fujifilm-Wako) and 0.27% acetic anhydride (Nacalai Tesque) for 10 min at room temperature. Then, specimens were treated with G1T0 followed by the mixture of antigen retrieval solution and prehybridization solution containing 3.78 M urea, 0.063 M Tris-HCl (pH = 9.5), 50  $\mu\text{g}/\text{mL}$  heparin, 100  $\mu\text{g}/\text{mL}$  yeast tRNA, and 1% Tween 20. Sense and antisense RNA probes of macho-1 were transcribed from a *Ciona* cDNA clone (cieg016n12: Ghost) [23], using T7 and T3 RNA polymerases (Sigma-Aldrich), respectively, with DIG RNA Labeling Mix (Sigma-Aldrich). The specimens were hybridized with an RNA probe in prehybridization buffer (50% formamide, 50  $\mu\text{g}/\text{mL}$  heparin, 100  $\mu\text{g}/\text{mL}$  yeast tRNA, and 1% Tween 20) for 16 h at  $50^{\circ}\text{C}$ . After hybridization, the specimens were washed with SSC ( $5\times$ ,  $2\times$ , and  $0.2\times$ ). For observation of macho-1, DIG probe was detected using an alkaline phosphatase-conjugated anti-DIG Fab fragment (Sigma-Aldrich; 1:1000 dilution). In contrast, when combined with immunofluorescence, specimens were immunostained with the following antibodies: anti-Bip rabbit polyclonal antibody, anti-NN18 mouse monoclonal antibody (antineurofilament antibody; Sigma-Aldrich; 1:100 dilution), horseradish peroxidase-conjugated anti-DIG Fab fragment (Sigma-Aldrich; 1:100 dilution), Alexa Fluor Plus 555-conjugated goat anti-rabbit IgG antibody, and Alexa Fluor 405-conjugated goat anti-mouse IgG antibody (Thermo Fisher Scientific; 1:200 dilution). The NN18 antibody is a good marker of mitochondria that recognizes the F1-ATP synthase  $\alpha$ -subunit in *Ciona* [24]. After immunostaining, the in situ hybridization signals were enhanced using FITC-Tyramide (Akoya Biosciences, Marlborough, MA, USA).

### 2.5. Image Acquisition and Data Analysis

Specimens were observed under LSM700 (Carl Zeiss, Jene, Germany) or A1RHD25 (Nikon, Tokyo, Japan) confocal microscopes using ZEN (Carl Zeiss) or NIS element imaging software (Nikon). Z-projections and the midplane optical sections are displayed with animal pole upward. The animal pole was defined based on the position of the meiotic apparatus, myoplasm configuration, or parallel direction of the CAMP [12]. All analyses were performed using the ImageJ software [25]. Z-projections were displayed as a side view wherein the animal pole was up and posterior side was right, or as a posterior view wherein the animal pole was up. These Z-projections showed the maximum intensity projection of z-stack. To analyze the expansion of the signal area of macho-1 mRNA, the angles between the horizontal and vertical edges of the mRNA signal and the center of the eggs were measured. For the measurement of angles, the side and top views of the Z-projections were used. To analyze the colocalization between the ER and mRNA signals, Z-projections were rendered from five optical sections around the midplane. Then, the dense ER region was extracted using denoising, contrast adjustment, and binarization, followed by a restriction of the object size. The maternal mRNA-positive region was extracted by binarization of the mRNA signals. The ratio of the mRNA-positive regions in the dense ER to the total area of mRNA-positive regions was calculated. The parameters for the extraction of each dense ER or mRNA were fixed for all specimens.

## 3. Results

### 3.1. Prolonged F-Actin Accumulation at the Vegetal Cortex

It has been well-described that the actin cytoskeleton is necessary for the first phase of ooplasmic segregation and results in strong F-actin accumulation in the vegetal cortex [9–11]. However, no report has described how long this accumulation lingered in the vegetal pole. Thus, we improved the phalloidin staining method for detecting F-actin in whole-mount specimens. The main points of this improvement were fixation with permeabilization and treatment with the fructose-based hydrophilic clearing reagent SeeDB [22]. Our methods revealed that vegetal accumulation of F-actin decreased gradually, though it was detected up to at least 30 mpf (Figure 1). The mitotic apparatus was faintly stained at 45 mpf (Figure 1b). As the meiotic spindles beneath the animal cap were not stained, this phalloidin staining of the microtubule structure suggests that the colocalization of actin and tubulin during the second phase of ooplasmic segregation is plausible.

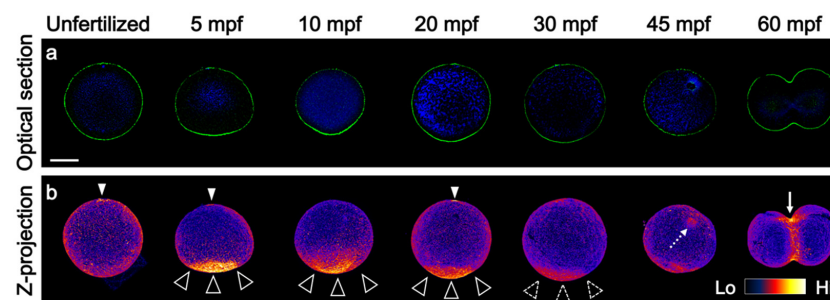


**Figure 1.** Duration of vegetally localized F-actin after fertilization. (a) The embryos during first cell cycle were stained for DNA (blue) and F-actin (green) by using 4',6-diamidino-2-phenylindole dihydrochloride (DAPI) and phalloidin. The optical sections of the midplane are shown except for 60 mpf. At 60 mpf, the frontal view wherein the animal pole is up and right side is right was shown, because the cleavage furrow can be easily observed in this plane. The timings of fixation are indicated on top. The F-actin significantly localized to the vegetal pole at least until 30 mpf. Closed arrowheads in 5 and 20 mpf indicate actin caps of polar body I and II, respectively, suggesting the existence of meiotic spindle beneath them [26]. These observations were repeated four times in each time point using approximately 50 eggs in each experiment. (b) Z-projection models were rendered from single channel of F-actin and represented in fire gradient. The range indicator is shown at the right corner. Arrowheads and dotted arrowheads indicate the strong and weak signals of F-actin at the vegetal pole, respectively. The staining of the other cortical region including 45 mpf was not obvious nor consistent. Mitotic apparatus was slightly stained in 45 mpf (dotted arrow) and contractile ring of cleavage furrow was brightly stained in 60 mpf (arrow). Animal pole (A) is up. Scale bar: 50  $\mu$ m.



### 3.2. Actin Depolymerization Induced Malformation of CAMP

To reveal the functions of prolonged F-actin accumulation at the vegetal cortex during the following events, eggs were treated with CytB at various periods during the first cell cycle; CytB\_01 (0 to 10 mpf), CytB\_02 (0 to 30 mpf), CytB\_03 (10 to 30 mpf), and CytB\_04 (30 to 45 mpf), as shown in Figure 2a. To investigate the effect of CytB treatment on axis formation, we analyzed the second phase of ooplasmic segregation extensively. The effect of CytB treatment was confirmed by phalloidin staining of normal eggs fixed at 10 mpf. In those eggs, no F-actin staining in the vegetal pole could be found (Figure 2b,b'). First, microtubule structures in the eggs of 45 mpf were observed. In the control egg, the CAMP was normally formed, representing a kind of convergence to the midline; thus, microtubule bundles were dense around the midline (Figure 2c). The CAMP formed by CytB\_01 and CytB\_03 treatments were relatively normal, though expanded broadly, and did not show midline accumulation of microtubule bundles (Figure 2d,f). The CytB\_02 treatment gave rise to a widely and randomly distributed microtubule network in the vegetal hemisphere (Figure 2e). In the CytB\_04 treatment, although the microtubule bundles were arrayed in a similar direction and accumulated around the postulated posterior pole, this CAMP-like structure was missing a large portion (Figure 2g). We supposed that the treatment with CytB before the second phase of ooplasmic segregation broadened the CAMP-forming area and made the anteroposterior axis ambiguous, whereas the treatment during the second phase of movement caused a defective CAMP with the postulated anteroposterior axis. Moreover, although several chromosomes detached from spindle microtubules in CytB\_02 (Figure 2j), mitotic apparatus for the first cleavage had bipolar spindles and asters in all CytB-treated eggs (Figure 2h–l). Thus, the effect of CytB treatment mainly affected the microtubules beneath the egg cortex, suggesting a relationship between microfilaments and microtubules beneath the egg cortex.

### 3.3. The Prolonged F-Actin Localization Contributed to the Midline Accumulation of Myoplasm and Maternal mRNA

As the effect of CytB on CAMP formation was different, we first focused on the effect before the second phase of ooplasmic segregation (0 to 30 mpf). The CytB-treated eggs were fixed at 45 mpf and triple-stained for macho-1 mRNA, ER, and mitochondria (Figure 3). In DMSO-treated control embryos, dense ER, MRC, and macho-1 were clearly localized and concentrated at the posterior pole, and both mitochondria and macho-1 were excluded from the dense ER region, as reported in our previous paper (Figure 3a,a',h). When eggs were treated with CytB, the distribution of macho-1 broadly expanded with various phenotypes (Figure 3b–d,b'–d',b''–d''). In CytB\_01, although a large part of macho-1 was localized to the posterior side, some macho-1 were left in anterior side (Figure 3b,b'). Moreover, the localized area of macho-1 was broadened along a left–right axis (Figure 3b''). This result might be due to the retention of macho-1 on almost the entire egg cortex caused by the inhibition of the first phase of ooplasmic segregation. In CytB\_02, macho-1 was broadly localized in the cortical regions of the vegetal hemisphere (Figure 3c,c',c''). This severe phenotype was thought to be the additive effect of CytB\_01 and CytB\_03. In most cases of CytB\_03, macho-1 moved and localized to the posterior pole, similar to those of the normal control (Figure 3d,d'), however, it showed wider distribution along the left–right axis (Figure 3d''). Notably, CytB\_01 and 02 treatments showed scattered distributions of macho-1 signals, while CytB\_03 treatment showed a single lump of macho-1 signal (Figure 3b''–d''). In the quantitative analyses of these results, it was clearly demonstrated that CytB treatments had different effects for the macho-1 distributions along the anteroposterior and left–right axes (Figure 3e–g). To summarize these results, depolymerization of F-actin during the first segregation movement resulted in the scattered and broadened localization of macho-1 along both anteroposterior and left–right axes, while the depolymerization of F-actin during the period between the first and second segregation only broadened the macho-1 localization along the left–right axis. Thus, it was suggested that the actin filaments during the first phase of segregation had the role of lumping macho-1

mRNAs into a single mass in addition to the constriction of the egg cortex into the vegetal pole, and prolonged localization of actin filaments beneath the vegetal pole had the role of the convergence of macho-1 mRNAs to the midline. The MRC resided adjacent to the inner side of dense ER, and macho-1 extruded from dense ER and into the MRC and deeper cytoplasm in all treatments (Figure 3h–k). Although, the macho-1 mRNA was distributed abnormally by CytB treatments, dense ER and MRC were situated close to macho-1, and MRC was always situated next to the dense ER.

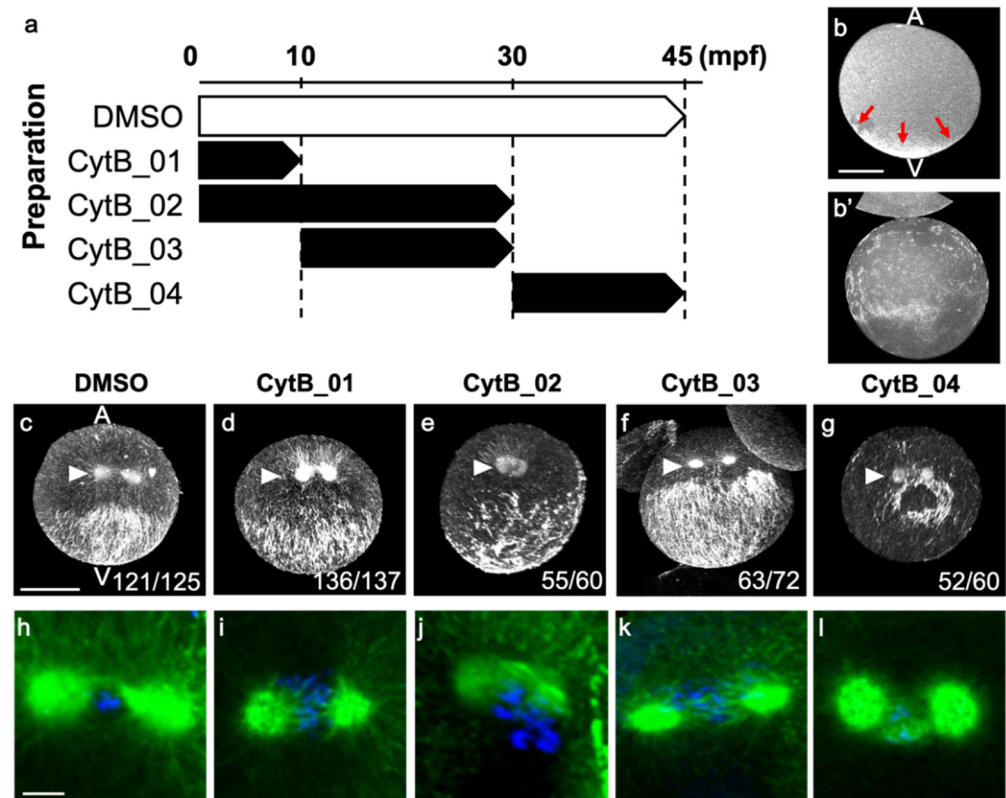


**Figure 2.** The effect of CytB treatment on CAMP formation during first cell cycle. (a) Schematic drawing of sample preparation. The white and black blocks indicate incubation periods with DMSO and 2 µg/mL CytB, respectively. The egg was treated with DMSO as the normal control. (b,b') Normal (b) and CytB-treated eggs (b') were fixed at 10 mpf and stained with phalloidin. CytB-treated eggs did not show F-actin staining in the vegetal pole. The Z-projections of the side view are shown. Animal pole (A) is up. Arrows indicate strong signal at the vegetal pole. Scale bar: 50 µm. (c–g) Eggs were fixed at 45 mpf and immunostained for tubulin. Preparation name of each egg is indicated on the top. Animal pole (A) is up. Posterior views of rendered Z-projection representing various malformations of CAMP. Normal CAMP emerges as a parallel array of microtubules on the posterior-vegetal cortex. Microtubule bundles are relatively dense around the midline (c). Arrowhead indicates mitotic apparatus of first cleavage, representing the midplane is situated in between two centrosomes. It should be noted that, although the progression of the cell cycle was slightly affected (d). The number of embryos represented by the image over the number of embryos examined is indicated at the right corner. Scale bar: 50 µm. (h–l) Enlarged Z-projections rendered from 30 optical sections around the mitotic apparatus in (c–g) are represented. Green and blue indicate microtubule and DNA, respectively. Scale bar: 10 µm.

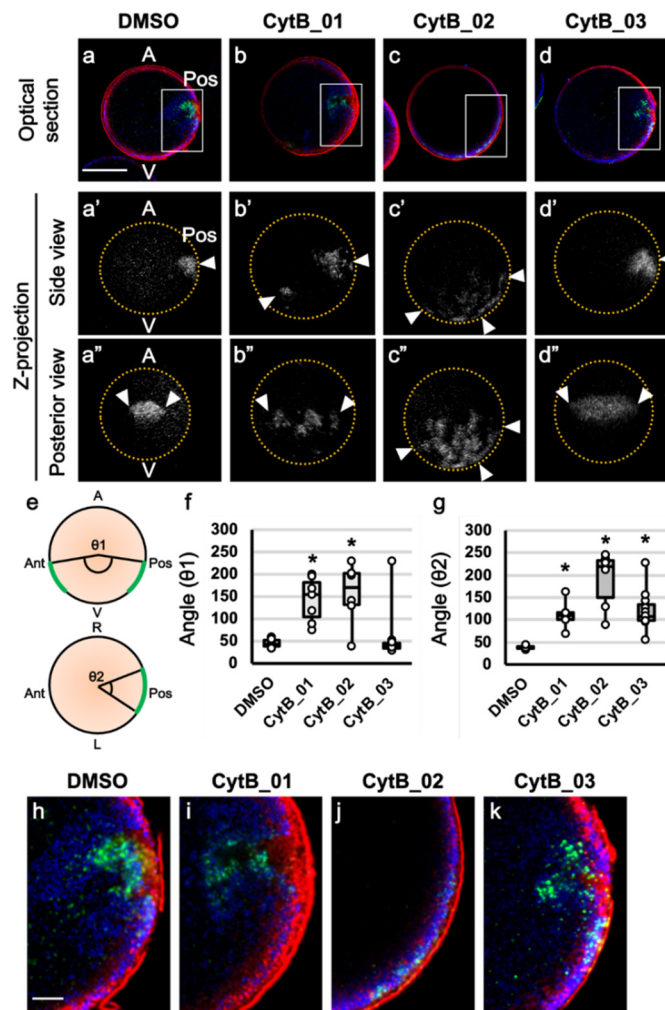


**Figure 3.** The role of prolonged F-actin localization to the vegetal cortex for translocations of organelles and maternal mRNA. (a–d,a'–d',a''–d'') The CytB-treated eggs were fixed at 45 mpf. Preparation of each egg is indicated on the top. The double-immunostaining of ER (red) and mitochondria (blue) and in situ hybridization of macho-1 (green) were carried out. Merged images of midplane optical sections ((a–d): optical section) and Z-projections of single channel of macho-1 are shown ((a'–d'): side view, (a''–d''): posterior view). Yellow dotted lines indicate the outline of eggs. Animal pole (A) is up, vegetal pole (V) is down, and posterior pole (Pos) is on the right. Arrowheads indicate mRNA localized region. Scale bar: 50  $\mu$ m. (e) The angles,  $\theta_1$  and  $\theta_2$ , were measured between vertical and horizontal edges of mRNA signal area, respectively, and the center of eggs using Z-projection as shown in the schema. In CytB\_01, macho-1 signals were left in the anterior side, and thus,  $\theta_1$  became relatively large in most cases. (f,g) The central angle of the macho-1-localized region was measured on Z-projection and represented using box plots. Numbers of specimens were 7, 7, 6, and 11 in DMSO, CytB\_01, \_02, and \_03, respectively. These angles represent expansion of macho-1 localization with CytB treatments. Statistical significance was calculated by one-way ANOVA followed by the Dunnett's test (SD in f: DMSO = 9.6, CytB\_01 = 50.2, CytB\_02 = 69.7, CytB\_03 = 58.4; SD in g: DMSO = 3.8, CytB\_01 = 30.9, CytB\_02 = 64.9, CytB\_03 = 43.7). Significant differences versus DMSO are represented by asterisks ( $p < 0.01$ ). (h–k) Enlarged images of white rectangles of (a–d) are represented. In DMSO and CytB\_01, MRC (blue) was adjacent to the inner side of dense ER (red), while in CytB\_02 and \_03, MRC and dense ER were mingled but represented discrete distribution (blue and red signals do not overlapped). Scale bar: 10  $\mu$ m.

### 3.4. The Role of F-Actin during the Second Phase of Ooplasmic Segregation

Eggs treated with CytB\_04 were fixed at 45 mpf and triple-stained for ER, mitochondria, and macho-1 (Figure 4). In normal eggs, dense ER thickened its localized area at the posterior pole region and tended to intrude into the inner cytoplasm by following the movement of sperm aster, and macho-1 was excluded from the ER and intruded into the MRC or even deeper cytoplasm of the posterior pole (Figure 4a,a',c,c'). In the CytB\_04-treated egg, both macho-1 and dense ER were situated on the posterior vegetal cortex (Figure 4b,b'). However, they formed a thin localized area sticking to the cortex, and most of the macho-1 signal colocalized with dense ER (Figure 4d,d'). To examine the role of microtubules in the macho-1 translocation during the second phase of ooplasmic segregation, eggs were treated with 2.5 µg/mL Noco from 30 to 45 mpf (Figure 4e-e'',f-f'''). Noco treatment inhibited the second phase of ooplasmic segregation. Thus, the myoplasm remained in the vegetal pole, and the anteroposterior axis was abolished. Although no microtubule staining was observed in Noco-treated eggs, there was a faint tubulin staining at the vegetal pole (Figure 4e,e'). Dense ER colocalized with this tubulin-staining region, suggesting a close relationship between the ER and microtubules (Figure 4e''). According to the triple-staining result, mutual positioning of the vegetally stained ER and MRC was basically the same as the normal positioning of 30 mpf (Figure 4f,f') and of the CytB\_04 treatment. The MRC resided adjacent to the inner side of dense ER (Figure 4f'''). Although dense ER showed a thin layer beneath the posterior cortex and did not move into the egg cytoplasm in CytB\_04 treatment, Noco treatment did not change dense ER and MRC distribution (Figure 4d,d',f,f',f'''). On the other hand, in Noco treatment, most of the macho-1 signals colocalized with dense ER, similarly to CytB\_04 (Figure 4d,d',f,f',f'''). Quantitative analysis of this abnormality in the translocation of macho-1 revealed a similar effect of both actin and tubulin depolymerizations (Figure 4g,h). As macho-1 dissociated from dense ER by 30 mpf in the normal condition [14], macho-1 went back to dense ER under the condition with each inhibitor. Although, there is a possibility that the depolymerization of microtubules indirectly affects the macho-1 translocation by aborting the movement of the second phase, both F-actin and microtubules were suggested to have some roles in preventing macho-1 being reassociated with dense ER during the second phase of movement.

### 3.5. F-Actin Contributed to the Cleavage Patterning during the First Cell Cycle

The effect of CytB treatment during the first cell cycle to the later cleavage was investigated, focusing on the establishment of the anteroposterior axis. The eggs treated with CytB were fixed at the 32-cell stage and stained for macho-1 (Figure 5). In normal 32-cell stage embryos, macho-1 was localized to the CAB region, which resides equally in the posterior-most vegetal small blastomere pair (B6.3 and B6.3; micromere), and defined the posterior pole (Figure 5a). When the eggs were treated with CytB at various periods of the one-cell stage, they showed various abnormal phenotypes. Two-thirds of the embryos of CytB\_01 treatment gave rise to the embryo with two macho-1-localized spots in the adjacent micromeres, predicting the establishment of the anteroposterior axis, but the sizes of the signal areas and micromeres were unequal (Figure 5b). On the other hand, one-third of CytB\_01-treated embryos had two macho-1 localized spots in two discontinuous blastomeres, which could not define their posterior pole (Figure 5b'). CytB\_02-treated embryos showed the most severe phenotype. Most of the embryos showed delayed and abnormal cleavage with no symmetrical pattern, even in the embryo with two macho-1 signals in neighboring blastomeres (Figure 5c,c'). Three-fourths of them had a single elongated signal situated unevenly in two blastomeres (Figure 5c'). The majority of the CytB\_03-treated embryos had two or three macho-1-localized spots in the equivalent-size blastomeres, and thus could not show the anteroposterior axis (Figure 5d,d'). However, half of the CytB\_04-treated embryos had two macho-1-localized spots with weak left-right symmetry. The other half had only one macho-1-localized spot with no left-right symmetry (Figure 5e,e').



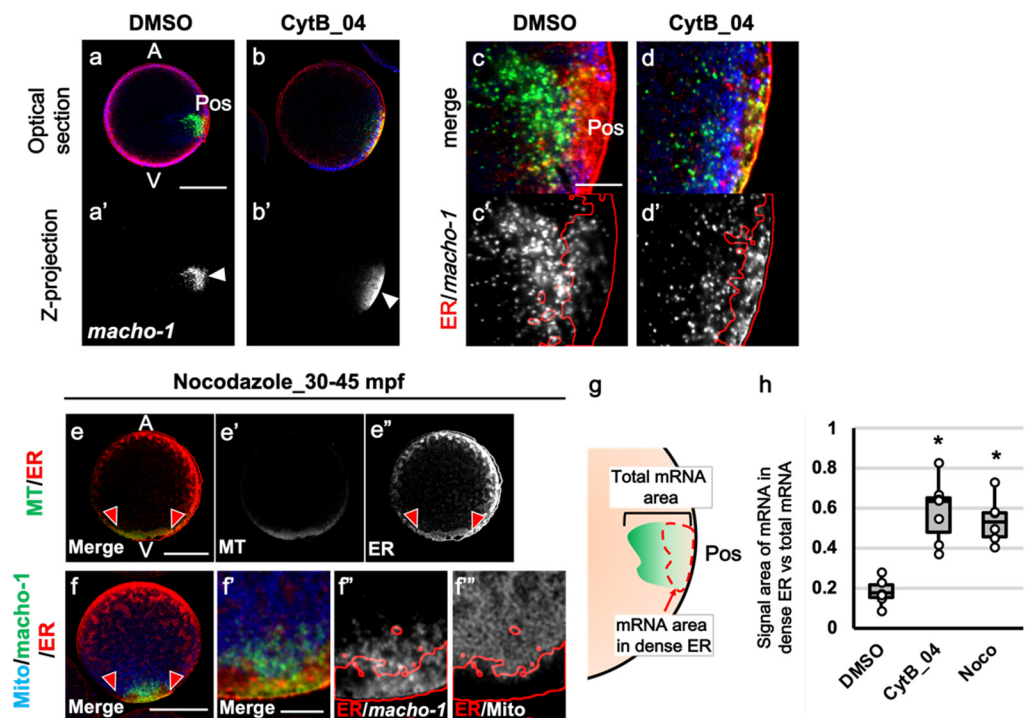


**Figure 4.** The role of F-actin during second phase of movement for the translocation of organelles and maternal mRNA. (a–d,a'–d') The CytB-treated eggs were fixed at 45 mpf and double-immunostaining of ER (red) and mitochondria (blue) and in situ hybridization of *macho-1* (green) were carried out. Preparation of each egg is indicated on the top. Merged images of midplane optical sections ((a,b): optical section) and rendered Z-projections of single channel of *macho-1* signal ((a',b'): Z-projection) are indicated. (c,d) Enlarged merged images of the posterior pole regions of a and b are shown (Merge). (c',d') The outline of dense ER region (red line) was superimposed on single channel of *macho-1* signal of c and d (white). Animal pole (A) is up, vegetal pole (V) is down, and posterior pole (Pos) is on the right. Arrowhead indicates *macho-1*-localized region. (e–e'',f–f'') Noco treatment was carried out during 30–45 mpf and fixed at 45 mpf. Single optical section of the plane including animal–vegetal axis are shown. Regions between two red arrowheads represent dense ER region. Noco-treated eggs were double stained for ER (red) and tubulin (MT; green). Merged images ((e): Merge) and single channel of each signal ((e'); MT, (e''); ER) are represented. Microtubule staining was not present, while faint staining was observed in vegetal pole region, presumably due to the tubulin monomer staining (e'). This tubulin staining was colocalized with dense ER (e,e''). Nocodazole-treated eggs were triple stained for ER (red)/mitochondria-rich cytoplasm (MRC; blue)/*macho-1* (green). Merged images (f: Merge) and enlarged image of vegetal pole region of f ((f'); Merge) are shown. Outlines of the dense ER region (red lines) were superimposed on in situ hybridization signals ((f''); ER/*macho-1*) and MRC signals ((f'''); ER/MRC). Note that the background ER staining of entire cortex of the egg became blotchy. Scale bars: 50  $\mu\text{m}$  (a,e,f) and 10  $\mu\text{m}$  (c,f'). (g) Colocalization between *macho-1* and dense ER was quantitatively evaluated by calculating the ratio of the signal area of the *macho-1* within the dense ER region to the total area of mRNAs, as shown in the schema. (h) The results of ratio of the *macho-1* signal area are represented using box plots. Dissociation of *macho-1* from dense ER was inhibited by both CytB<sub>04</sub> and Noco treatments. The number of specimens was 6 in all treatments. Statistical significance was calculated by one-way ANOVA followed by the Dunnett's test (SD: DMSO = 0.07, CytB<sub>04</sub> = 0.15, Noco = 0.11). Significant differences versus DMSO are represented by asterisks ( $p < 0.01$ ).

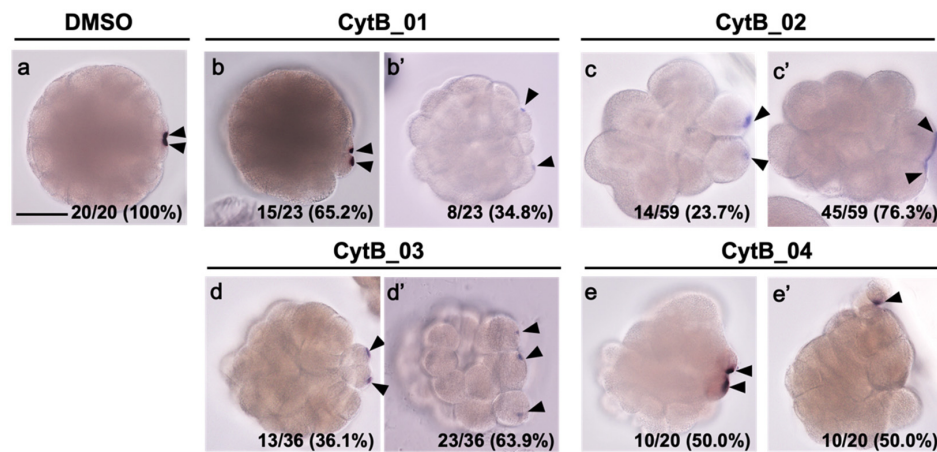


**Figure 5.** The effect of CytB treatment during 1-cell stage on the macho-1 mRNA localization. Preparation name of each egg is indicated on the top. Embryos were fixed at the 32-cell stage (about 3 h after fertilization) and stained for macho-1 by in situ hybridization. (a) The embryo treated with DMSO during 1-cell stage as a normal control exhibited two spots of macho-1 localization, which correspond to the CAB. The CAB is formed bilaterally in the posterior-most blastomeres of vegetal hemisphere, indicating the posterior pole. (b–e, b’–e’) The CytB-treated embryos represented cell-cycle retardation and various abnormal phenotypes. They were categorized into two types. In one phenotype, two CABs were formed in two neighboring blastomeres, suggesting the establishment of anteroposterior axis (b–e). The other type included the following phenotypes showing no obvious anteroposterior axis: two CABs were formed in separated blastomeres (b’), elongated CAB was asymmetrically inherited in two blastomeres (c’), three or more CABs were formed in separated blastomeres (d’), and a single CAB was formed in a random position of single blastomere (e’). Arrowheads indicate CABs. The number of embryos represented by the image over the number of embryos examined is indicated in the right corner. Scale bars: 50  $\mu$ m.

These embryos were then stained for macho-1 mRNA, ER, and mitochondria to observe their relative locations (Figure 6). In normal 32-cell stage embryos, macho-1 mRNA colocalized with ER in the micromeres corresponding to CAB formation (Figure 6a, a’). Although CytB-treated embryos showed an abnormal distribution pattern of macho-1 after the second phase of ooplasmic segregation, localized spots of macho-1 in all the treatments were colocalized with ER, suggesting that CAB formation normally occurred (Figure 6b–g, b’–g’). As shown in Figure 5, some of the CABs did not lead to unequal cleavage and posterior pole formation. These CABs suggested a lack of some factors, which is inevitable for exerting the complete function of CAB. Our results suggested that depolymerization of F-actin during the first cell cycle affects the formation of normal CAB.

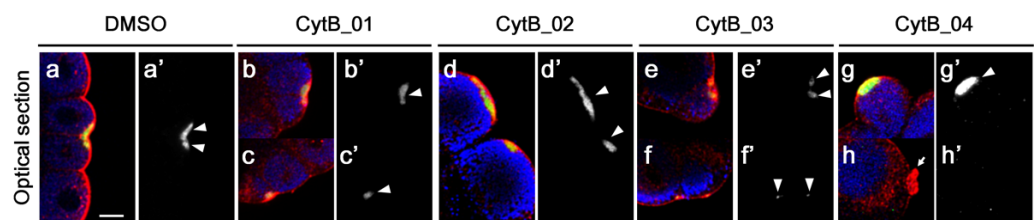


**Figure 6.** Colocalization of macho-1 with ER on the CAB at 32-cell stage. Embryos treated with CytB were fixed at 32-cell stage. The double-immunostaining of ER (red) and mitochondria (blue) and in situ hybridization of macho-1 (green) were performed. (a–h) Single optical section of merged images of CAB region. (a’–h’) Single channel of macho-1 in (a–h). Preparation name of each egg is indicated on the top. macho-1 and ER were colocalized at all the CAB regions (arrowheads) despite the CytB treatment. Only the CytB\_04-treated embryo represented small debris of ER, which did not contain macho-1 (arrow). Scale bar: 10  $\mu$ m.

### 3.6. The Disordered Morphogenesis Induced by Cytb Treatment during First-Cell Cycle

Finally, to examine the effect of CytB treatment during the first cell cycle on normal CAB formation, the larval phenotype was examined (Figure 7). Normal larva represented a tadpole shape with a trunk and long tail representing obvious anteroposterior axis (Figure 7a). All of the CytB treatments led to abnormal development and gave rise to two phenotypes (Figure 7b–e, b'–e'). In one phenotype, irregular trunk and abnormal short tail could be identified, suggesting anteroposterior axis formation. In some cases, a pigment granule (thought to be an otolith according to its round shape) was developed (Figure 7b,e). This type of larvae developed approximately 60%, 25%, 45%, and 55% in CytB\_01, CytB\_02, CytB\_03, and CytB\_04, respectively (Figure 7b'–e'). These proportions were close to those of the 32-cell stage embryo with left–right symmetry, as shown in Figure 5. In the other phenotype, although the secretion of tunic suggesting epidermal development and faint rotation symmetry could be observed, it was a type of cell aggregate and we could not define the anteroposterior axis (Figure 7b'–e'). These embryos were thought to be developed from the 32-cell-stage embryo with no anteroposterior axis (Figure 5). This result implied that some CABs could not exert complete functions nor define the anteroposterior axis, suggesting that some important factors were missing from CAB by CytB treatment.

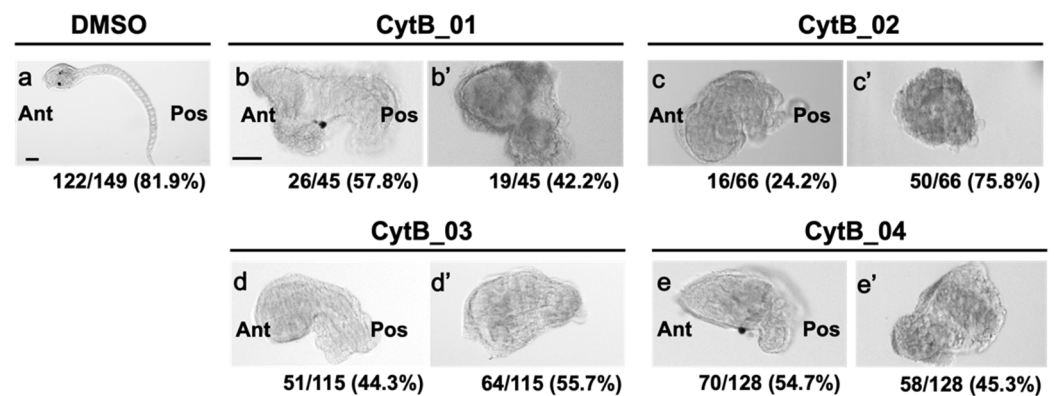


**Figure 7.** The effect of CytB treatment during the 1-cell stage on the larval morphogenesis. Preparation name of each egg is indicated on the top. Embryos were fixed at 20 h postfertilization. (a) The embryo treated with DMSO during 1-cell stage as a normal control exhibited tadpole shape, which has trunk and tail representing anterior (Ant)–posterior (Pos) axis. In addition, two pigment spots (otolith and ocellus) were developed. (b–e, b'–e') The CytB-treated embryos represented various abnormal morphologies. They were categorized into two types. In one type, trunk and tail could be distinguished, suggesting the establishment of anterior–posterior axis. In some cases, otolith-like pigment granules could be observed (b,e). In the other type, embryos became cell aggregates and had no anteroposterior axis. Although they seemed to have tunic on their surface, no other obvious tissue differentiation could be observed (b'–e'). The number of embryos represented by the image over the number of embryos examined is indicated at the right corner. Scale bars: 50  $\mu$ m.

## 4. Discussion

Owing to the methods using unique fixation and hydrophilic clearing reagents, we found prolonged actin localization to the vegetal pole until the start of the second phase. Moreover, we analyzed the role of F-actin during the first cell cycle by describing the colocalization of ER, mitochondria, and mRNA.

When F-actin was depolymerized by CytB at various periods, the cortical microtubule structure, CAMP, showed abnormal shapes according to the period of CytB treatment. The common phenotype of the depolymerization of prolonged vegetal F-actin was the laterally broadened CAMP area, suggesting the inhibition of the convergence of microtubule bundles to the midline. The function and localization of F-actin during the first cell cycle of ascidian early development were reported mainly on the first phase of ooplasmic segregation [9–11], except for a few reports on the existence of cortical F-actin in the posterior–vegetal cortex

during the second phase [27], which we could not confirm in our experiment. Thus, this is the first report that F-actin has some roles, in addition to the first phase of ooplasmic segregation. Specifically, in this report, we found three different roles for maternal mRNA translocation in three different periods, during the first phase of movement, the period between first and second phase, and the second phase of movement. During the first phase, a cortically distributed actin network was suggested to have a role for lumping maternal mRNA in addition to generating contracting force of the first segregation movement. During the period between first and second segregation, prolonged vegetal cortex F-actin was closely located to the vegetally accumulated microtubule fragment [13] and had a role in the convergence of mRNA, mitochondria, and ER to the midline. During the second phase, although we could not detect cortical actin network, depolymerization of F-actin affected the CAMP formation and relocation of maternal mRNA to the dense ER region. The role for keeping maternal mRNAs dissociated from ER was shared by microtubules. These close relationships between microfilaments and microtubules strongly suggest their collaborative mechanisms.

The collaborative role of actin and tubulin in CAMP formation is not an inconceivable event, as it has been reported that actin filaments in somatic cells have various functions in microtubule organization, such as anchoring to the cortex and directional elongation [28]. Moreover, CAMP is suggested to be an acentrosomal microtubule structure. It has been reported that the acentrosomal microtubule structure could be regulated by actin through the spectraplakins (ACF7; crosslinking cytoskeletal protein by binding to both microtubules and F-actin) and the microtubule end-binding proteins (CAMSAP3: calmodulin-regulated spectrin-associated protein 3) [29]. Thus, to reveal the interaction between actin and microtubule in the ascidian egg, analyses of these cytoskeletal-associated molecules are necessary.

The macho-1 dissociation from dense ER during the second phase of ooplasmic segregation was another collaborative mechanism of actin and tubulin. It is well-known that both microtubules and microfilaments have a role in trafficking mRNP granules, complexes of mRNA and ribonucleoproteins (e.g., [30]). In budding yeast, it has been reported that the localization of polysome-interacting protein on the ER is regulated by microtubules [31]. In *Ciona* eggs, one of the RNA binding proteins, Y-box binding protein (YB-1), interacts with *pem-1* mRNA, suggesting the existence of mRNP granule [32]. Type I postplasmic/PEM RNAs associate with ribosomes, which are localized to the cER [33]. From the viewpoint of the collaborative role of different cytoskeletal filaments, an intangible molecular mechanism emerges by combining these reports. In this mechanism, translocation of organelles and mRNA are closely related to translational control. In our results, the importance of excluding mRNA from dense ER is cryptic, whereas the collaborative participation of two different cytoskeletal filaments is a promising mechanism for understanding the translocation of maternal determinants.

On the other hand, the malformation of microtubule structure and the mislocalization of mRNA caused by the depolymerization of microfilaments during the first cell cycle largely affected early development by spoiling the anteroposterior axis. Although most of these damaged embryos had CABs, they could not exert their complete functions, such as determination of the posterior pole and unequal cleavage. This suggested that the components of CABs formed in damaged embryos were insufficient. A considerable number of molecules have been revealed, such as about 40 postplasmic/PEM RNAs and their translational products, Kinesin,  $\beta$ -catenin, YB-1, and regulators of translation initiation [7,16,32,34–37]. Thus, more detailed analyses including these CAB components are required for understanding the relationship between dysfunction of CAB and incomplete translocation of myoplasm. It is well-known that the correct transport of myoplasm and the appropriate distribution of the myoplasmic components through the ooplasmic segregation are important for ascidian development. According to our results, we believe that the precise mechanisms of ooplasmic segregation are more complicated than ever thought. The collaborative role of microfilaments and microtubules is one of these complexities. More



extensive analyses of the mechanisms underlying ooplasmic segregation will contribute to the understanding of the molecular mechanisms of ascidian embryogenesis.

**Author Contributions:** T.G. designed the study, performed the experiments, quantitative analysis, and original draft preparation; S.T., A.K. and K.K. performed the experiments and supported the quantitative analysis; J.K. and Y.K. conceived of this study and participated in interpretation of data; T.N. contributed to the conception of this study and helped to draft the manuscript. All authors have read and agreed to the published version of the manuscript.

**Funding:** This research did not receive any specific grants from funding agencies in the public, commercial, or not-for-profit sectors.

**Institutional Review Board Statement:** Not applicable.

**Informed Consent Statement:** Not applicable.

**Data Availability Statement:** The datasets generated and/or analyzed during the current study are available from the corresponding author upon reasonable request.

**Acknowledgments:** We would like to thank Shirae-Kurabayashi, M. (Nagoya University, Japan) for valuable discussions on immunostaining methods and in situ hybridization. We thank the National BioResource Project for providing *Ciona intestinalis*.

**Conflicts of Interest:** The authors have no conflict of interest directly relevant to the content of this article.

## References

1. Miller, J.R.; Rowning, B.A.; Larabell, C.A.; Yang-Snyder, J.A.; Bates, R.L.; Moon, R.T. Establishment of the Dorsal–Ventral Axis in *Xenopus* Embryos Coincides with the Dorsal Enrichment of Dishevelled that Is Dependent on Cortical Rotation. *J. Cell Biol.* **1999**, *146*, 427–438. [[CrossRef](#)]
2. Tao, Q.; Yokota, C.; Puck, H.; Kofron, M.; Birsoy, B.; Yan, D.; Asashima, M.; Wylie, C.C.; Lin, X.; Heasman, J. Maternal Wnt11 Activates the Canonical Wnt Signaling Pathway Required for Axis Formation in *Xenopus* Embryos. *Cell* **2005**, *120*, 857–871. [[CrossRef](#)] [[PubMed](#)]
3. Tran, L.D.; Hino, H.; Quach, H.; Lim, S.; Shindo, A.; Mimori-Kiyosue, Y.; Mione, M.C.; Ueno, N.; Winkler, C.; Hibi, M.; et al. Dynamic Microtubules at the Vegetal Cortex Predict the Embryonic Axis in Zebrafish. *Development* **2012**, *139*, 3644–3652. [[CrossRef](#)] [[PubMed](#)]
4. Lyczak, R.; Gomes, J.E.; Bowerman, B. Heads or Tails: Cell Polarity and Axis Formation in the Early *Caenorhabditis Elegans* Embryo. *Dev. Cell* **2002**, *3*, 157–166. [[CrossRef](#)]
5. Nance, J.; Zallen, J.A. Elaborating Polarity: PAR Proteins and the Cytoskeleton. *Development* **2011**, *138*, 799–809. [[CrossRef](#)] [[PubMed](#)]
6. Sardet, C.; Nishida, H.; Prodon, F.; Sawada, K. Maternal mRNAs of PEM and Macho 1, the Ascidian Muscle Determinant, Associate and Move with a Rough Endoplasmic Reticulum Network in the Egg Cortex. *Development* **2003**, *130*, 5839–5849. [[CrossRef](#)]
7. Prodon, F.; Yamada, L.; Shirae-Kurabayashi, M.; Nakamura, Y.; Sasakura, Y. Postplasmic/PEM RNAs: A Class of Localized Maternal mRNAs with Multiple Roles in Cell Polarity and Development in Ascidian Embryos. *Dev. Dyn.* **2007**, *236*, 1698–1715. [[CrossRef](#)]
8. Sardet, C.; Paix, A.; Prodon, F.; Dru, P.; Chenevert, J. From Oocyte to 16-Cell Stage: Cytoplasmic and Cortical Reorganizations that Pattern the Ascidian Embryo. *Dev. Dyn.* **2007**, *236*, 1716–1731. [[CrossRef](#)] [[PubMed](#)]
9. Sawada, T.-O.; Schatten, G. Effects of Cytoskeletal Inhibitors on Ooplasmic Segregation and Microtubule Organization during Fertilization and Early Development in the Ascidian *Molgula Occidentalis*. *Dev. Biol.* **1989**, *132*, 331–342. [[CrossRef](#)]
10. Chiba, S.; Miki, Y.; Ashida, K.; Wada, M.R.; Tanaka, K.J.; Shibata, Y.; Nakamori, R.; Nishikata, T. Interactions Between Cyto-Skeletal Components during Myoplasm Rearrangement in Ascidian Eggs. *Dev. Growth Differ.* **1999**, *41*, 265–272. [[CrossRef](#)]
11. Roegiers, F.; Djediat, C.; Dumollard, R.; Rouviere, C.; Sardet, C. Phases of Cytoplasmic and Cortical Reorganizations of the Ascidian Zygote between Fertilization and First Division. *Development* **1999**, *126*, 3101–3117. [[CrossRef](#)] [[PubMed](#)]
12. Ishii, H.; Goto, T.; Nishikata, T. Microtubule Array Observed in the Posterior-Vegetal Cortex during Cytoplasmic and Cortical Reorganization of the Ascidian Egg. *Dev. Growth Differ.* **2017**, *59*, 648–656. [[CrossRef](#)] [[PubMed](#)]
13. Goto, T.; Kanda, K.; Nishikata, T. Non-Centrosomal Microtubule Structures Regulated by Egg Activation Signaling Contribute to Cytoplasmic and Cortical Reorganization in the Ascidian Egg. *Dev. Biol.* **2018**, *448*, 161–172. [[CrossRef](#)]
14. Goto, T.; Torii, S.; Kondo, A.; Kawakami, J.; Yagi, H.; Suekane, M.; Kataoka, Y.; Nishikata, T. Dynamic Changes in the Association between Maternal mRNAs and Endoplasmic Reticulum during Ascidian Early Embryogenesis. *Dev. Genes Evol.* **2021**, 1–14. [[CrossRef](#)]

15. Hibino, T.; Nishikata, T.; Nishida, H. Centrosome-Attracting Body: A Novel Structure Closely Related to Unequal Cleavages in the Ascidian Embryo. *Dev. Growth Differ.* **1998**, *40*, 85–95. [[CrossRef](#)]
16. Nishikata, T.; Hibino, T.; Nishida, H. The Centrosome-Attracting Body, Microtubule System, and Posterior Egg Cytoplasm Are Involved in Positioning of Cleavage Planes in the Ascidian Embryo. *Dev. Biol.* **1999**, *209*, 72–85. [[CrossRef](#)]
17. Ishii, H.; Kunihiro, S.; Tanaka, M.; Hatano, K.; Nishikata, T. Cytosolic Subunits of ATP Synthase are Localized to the Cortical Endoplasmic Reticulum-Rich Domain of the Ascidian Egg Myoplasm. *Dev. Growth Differ.* **2012**, *54*, 753–766. [[CrossRef](#)] [[PubMed](#)]
18. Ishii, H.; Shirai, T.; Makino, C.; Nishikata, T. Mitochondrial Inhibitor Sodium Azide Inhibits the Reorganization of Mitochondria-Rich Cytoplasm and the Establishment of the Anteroposterior Axis in Ascidian Embryo. *Dev. Growth Differ.* **2014**, *56*, 175–188. [[CrossRef](#)] [[PubMed](#)]
19. Ojima, K.; Lin, Z.X.; Andrade, I.R.; Costa, M.L.; Mermelstein, C. Distinctive Effects of Cytochalasin B in Chick Primary Myoblasts and Fibroblasts. *PLoS ONE* **2016**, *11*, e0154109. [[CrossRef](#)]
20. Hayashi, T.; Lewis, A.; Hayashi, E.; Betenbaugh, M.J.; Su, T.P. Antigen Retrieval to Improve the Immunocytochemistry Detection of Sigma-1 Receptors and ER Chaperones. *Histochem. Cell Biol.* **2011**, *135*, 627–637. [[CrossRef](#)]
21. Prodon, F.; Hanawa, K.; Nishida, H. Actin Microfilaments Guide the Polarized Transport of Nuclear Pore Complexes and the Cytoplasmic Dispersal of Vasa mRNA during GVBD in the Ascidian *Halocynthia roretzi*. *Dev. Biol.* **2009**, *330*, 377–388. [[CrossRef](#)]
22. Ke, M.-T.; Fujimoto, S.; Imai, T. SeeDB: A Simple and Morphology-Preserving Optical Clearing Agent for Neuronal Circuit Reconstruction. *Nat. Neurosci.* **2013**, *16*, 1154–1161. [[CrossRef](#)]
23. Satou, Y.; Satoh, N. Cataloging Transcription Factor and Major Signaling Molecule Genes for Functional Genomic Studies in *Ciona intestinalis*. *Dev. Genes Evol.* **2005**, *215*, 580–596. [[CrossRef](#)]
24. Chenevert, J.; Pruliere, G.; Ishii, H.; Sardet, C.; Nishikata, T. Purification of Mitochondrial Proteins HSP60 and ATP Synthase from Ascidian Eggs: Implications for Antibody Specificity. *PLoS ONE* **2013**, *8*, e52996. [[CrossRef](#)]
25. Schindelin, J.; Arganda-Carreras, I.; Frise, E.; Kaynig, V.; Longair, M.; Pietzsch, T.; Preibisch, S.; Rueden, C.; Saalfeld, S.; Schmid, B.; et al. Fiji: An Open-Source Platform for Biological-Image Analysis. *Nat. Methods* **2012**, *9*, 676–682. [[CrossRef](#)] [[PubMed](#)]
26. McDougall, A.; Hebras, C.; Pruliere, G.; Burgess, D.; Costache, V.; Dumollard, R.; Chenevert, J. Role of PB1 Midbody Remnant Creating Tethered Polar Bodies during Meiosis II. *Genes* **2020**, *11*, 1394. [[CrossRef](#)]
27. Jeffery, W.R.; Meier, S. A Yellow Crescent Cytoskeletal Domain in Ascidian Eggs and its Role in Early Development. *Dev. Biol.* **1983**, *96*, 125–143. [[CrossRef](#)]
28. Dogterom, M.; Koenderink, G.H. Actin–Microtubule Crosstalk in Cell Biology. *Nat. Rev. Mol. Cell Biol.* **2018**, *20*, 38–54. [[CrossRef](#)]
29. Noordstra, I.; Liu, Q.; Nijenhuis, W.; Hua, S.; Jiang, K.; Baars, M.; Rimmelzwaal, S.; Martin, M.; Kapitein, L.C.; Akhmanova, A. Control of Apico-Basal Epithelial Polarity by the Microtubule Minus-End Binding Protein CAMSAP3 and Spectraplakins ACF7. *J. Cell Sci.* **2016**, *129*, 4278–4288. [[CrossRef](#)] [[PubMed](#)]
30. Koppers, M.; Özkan, N.; Fariás, G.G. Complex Interactions between Membrane-Bound Organelles, Biomolecular Condensates and the Cytoskeleton. *Front. Cell Dev. Biol.* **2020**, *8*, 1661. [[CrossRef](#)] [[PubMed](#)]
31. Frey, S.; Pool, M.; Seedorf, M. Scp160p, an RNA-Binding, Polysome-Associated Protein, Localizes to the Endoplasmic Reticulum of *Saccharomyces cerevisiae* in a Microtubule-Dependent Manner. *J. Biol. Chem.* **2001**, *276*, 15905–15912. [[CrossRef](#)]
32. Tanaka, K.J.; Matsumoto, K.; Tsujimoto, M.; Nishikata, T. CiYB1 Is a Major Component of Storage mRNPs in Ascidian Oocytes: Implications in Translational Regulation of Localized mRNAs. *Dev. Biol.* **2004**, *272*, 217–230. [[CrossRef](#)]
33. Paix, A.; Yamada, L.; Dru, P.; Lecordier, H.; Pruliere, G.; Chenevert, J.; Satoh, N.; Sardet, C. Cortical Anchorages and Cell Type Segregations of Maternal Postplasmic/PEM RNAs in Ascidians. *Dev. Biol.* **2009**, *336*, 96–111. [[CrossRef](#)] [[PubMed](#)]
34. Costache, V.; Hebras, C.; Pruliere, G.; Besnardeau, L.; Failla, M.; Copley, R.R.; Burgess, D.; Chenevert, J.; McDougall, A. Kif2 Localizes to a Subdomain of Cortical Endoplasmic Reticulum that Drives Asymmetric Spindle Position. *Nat. Commun.* **2017**, *8*, 1–13. [[CrossRef](#)] [[PubMed](#)]
35. Negishi, T.; Takada, T.; Kawai, N.; Nishida, H. Localized PEM mRNA and Protein Are Involved in Cleavage-Plane Orientation and Unequal Cell Divisions in Ascidians. *Curr. Biol.* **2007**, *17*, 1014–1025. [[CrossRef](#)] [[PubMed](#)]
36. Kumano, G.; Nishida, H. Patterning of an Ascidian Embryo along the Anterior–Posterior Axis through Spatial Regulation of Competence and Induction Ability by Maternally Localized PEM. *Dev. Biol.* **2009**, *331*, 78–88. [[CrossRef](#)]
37. Paix, A.; Le Nguyen, P.N.; Sardet, C. Bi-Polarized Translation of Ascidian Maternal mRNA Determinant Pem-1 Associated with Regulators of the Translation Machinery on Cortical Endoplasmic Reticulum (cER). *Dev. Biol.* **2011**, *357*, 211–226. [[CrossRef](#)]